frontiers | Frontiers in Materials

ORIGINAL RESEARCH
published: 06 July 2022
doi: 10.3389/fmats.2022.913151

Co-Calcination of Bauxite Residue With Kaolinite in Pursuit of a Robust and High-Quality Supplementary Cementitious Material

Arne Peys[1]*, *Tobias Hertel*[2] *and Ruben Snellings*[1]

[1]Sustainable Materials, VITO, Mol, Belgium, [2]KU Leuven Department of Materials Engineering, Leuven, Belgium

The present article investigates the potential of co-calcination with kaolinite as a sector-wide solution for the transformation of bauxite residue into an effective supplementary cementitious material (SCM). Bauxite residues from eight alumina refineries were co-calcined with 30 wt% of kaolinite at 750°C. SCMs with moderately high reactivities were obtained. Mortars with 30 wt% replacement of Portland cement (CEM I) by co-calcined bauxite residue had relative strengths of 73 ± 4%, 87 ± 4%, and 88 ± 2% after 2, 7, and 28 days compared to a CEM I reference mortar. The reactivity and contribution to strength development were shown to scale linearly with the kaolinite dosage. Most bauxite residues require only 20 wt% substitution by kaolinite to reach the reactivity and performance targets. Co-calcination reduced the mobility of heavy metals significantly. The negative effect on the workability that some BRs with higher content of free sodium exhibited was mitigated by co-calcination. This positive effect was also observed after calcination with 10 and 20 wt% of kaolinite. The same was found for the positive effect on the leaching of heavy metals. The inherent reactivity of the bauxite residue mainly stemmed from the desilication products such as sodalite and cancrinite. During co-calcination, the sodium-containing phases reacted with kaolinite, delivering a supplementary cementitious material with high reactivity and low free-sodium content.

Keywords: bauxite residue, red mud, kaolinite, calcination, calcined clay, supplementary cementitious material, cement

OPEN ACCESS

Edited by:
Hung Quoc Nguyen, Vietnamese-German University, Vietnam

Reviewed by:
Jun Ren, Yunnan University, China
Zhuqing Yu, Nanjing Tech University, China

***Correspondence:**
Arne Peys
arne.peys@vito.be

Specialty section:
This article was submitted to Structural Materials, a section of the journal Frontiers in Materials

Received: *05 April 2022*
Accepted: *23 May 2022*
Published: *06 July 2022*

Citation:
Peys A, Hertel T and Snellings R (2022) Co-Calcination of Bauxite Residue With Kaolinite in Pursuit of a Robust and High-Quality Supplementary Cementitious Material. Front. Mater. 9:913151. doi: 10.3389/fmats.2022.913151

INTRODUCTION

The production of alumina is associated with the co-production of bauxite residue (BR). Most alumina refineries in the world use the Bayer process in which bauxite ore is leached with NaOH (Power et al., 2011; Evans 2016). While the main product of these refineries is aluminum hydroxide ($Al(OH)_3$ or $Al_2O_3.3H_2O$), which results in alumina (Al_2O_3) after calcination, a solid residue is obtained, named bauxite residue (BR), also known as red mud. The world's production of alumina was 134 million tons in 2020 (IAI 2021). The world's average BR production is approximately 1.35 ton alumina (Evans 2016), resulting in nearly 170 million ton production of BR in 2021. In 2017, the global production of BR was estimated to be 159 million tons (IAI 2020). In Europe, more specifically, the production of alumina was approximately 10.1 million tons in 2020 (IAI 2021) with an average BR/alumina ratio of 0.67 ton (Evans 2016), resulting in an estimated 6.8 million tons of BR in 2020. The utilization rate of BR is estimated at less than 3% (Power et al., 2011; Evans 2016)

and the most used application is in the production of Portland cement clinker as an addition to the raw meal (IAI 2020). Other possible applications are the production of iron and steel, the capping of landfills, road construction, and soil amelioration (Power et al., 2011; Evans 2016); however, the cement sector is selected as the most promising target market for high-volume application of BR by the International Aluminium Institute (IAI 2020). The production of cement in 2020 was 4,100 million tons globally (Garside 2021), of which, 4.3% was in the EU for an estimate of 176 million tons (CEMBUREAU 2020). Considering that a realistic cement replacement level by BR as an SCM could be 20–30 wt%, the entire annual BR production could be absorbed by the cement industry at the European and global levels.

The cement industry is facing increasing shortages of traditional supplementary cementitious materials (SCMs) such as coal, fly ash, and blast furnace slag (Juenger et al., 2019; Habert et al., 2020). The sustainable transition of the energy sector, in a planned phase-out, away from coal combustion in most European countries, will result in a decreased production of fly ashes (Taylor 2021). On the other hand, ground-granulated blast furnace slags (GGBFS) from pig iron production are highly desired because of their beneficial influence on cement performance, durability, and sustainability. For this reason, demand outstrips supply, resulting in high prices and lower clinker replacement rates on the level of a country or region than what is technically possible or environmentally optimal. The growing demand for new SCMs has been mentioned in many sustainability reports as a route to decrease the CO_2 output of the construction industry in the short term (Scrivener et al., 2016; Monteiro et al., 2017; Habert et al., 2020; Pamenter and Myers 2021). Many primary and secondary resources are under investigation for use as SCM; a few examples are calcined clays (e.g., with 40 wt% kaolinite), biomass ashes, municipal solid waste incinerator ashes, steel slags, slags from the non-ferrous metal industries, waste glass, mine tailings, spent pot lining, and BR (Aubert et al., 2006; Mladenovič et al., 2016; Scrivener et al., 2018; Bouchikhi et al., 2019; Juenger et al., 2019; Ohenoja et al., 2019; Danner and Justnes 2020; Hallet et al., 2020; Simonsen et al., 2020; Peys et al., 2021).

The use of BR as SCM has led to conflicting results when comparing several references in terms of compressive strength. Literature data show that a 20 wt% replacement of CEM I in mortars is associated with a significant 28 days of strength loss, similar to inert fillers (Danner and Justnes 2020) or worse (Serdar et al., 2017). This is in stark contrast with Ribeiro et al. (Ribeiro et al., 2010) and Venkatesh et al. (Venkatesh et al., 2020), where an increase in strength was observed for small additions and where a similar performance as the reference Portland cement is observed with up to at least 20 wt% cement replacement. Considering the chemical composition, the BRs of Ribeiro et al. (Ribeiro et al., 2010) and Venkatesh et al. (Venkatesh et al., 2020) seem to be more aluminum-rich and iron-poor than average, which might explain the better performance. However, there are not sufficient comparable literature data to draw decisive conclusions. Consensus can be found in the literature on the effect of BR on the workability and setting time. The cement hydration reactions are accelerated by the alkalinity of BR coming from the residual sodium from the Bayer process, lowering the setting time of mortars and concrete (Ribeiro et al., 2010; Serdar et al., 2017; Romano et al., 2018; Danner and Justnes 2020). The workability is negatively influenced by the addition of BR due to its soluble sodium content and fineness, which increase the superplasticizer need for concrete significantly compared to a reference concrete with fly ash as SCM (Tang et al., 2019). The environmental compatibility and mobility of heavy metals in cementitious products made with BR is not widely published, although BR is known to contain potentially hazardous elements such as Cr, As, or V (Evans 2016; IAI 2020).

The calcination of BR has been investigated as a means to improve its performance as SCM. Calcination was shown especially useful for boosting the reactivity of clays, leading to the potential for high cement replacement levels in limestone-calcined clay (LC^3) cements (Scrivener et al., 2019). Similarly, but not as extensive as for clay, the reactivity of BR can be improved using a calcination process (Ribeiro et al., 2013; Manfroi et al., 2014), if the calcination temperature is not too high (<800°C). The negative influence on the workability of mortars seems to be partially improved after calcination (Manfroi et al., 2014). A synergy was discovered by Danner et al. (Danner and Justnes 2020), who calcined a blend of BR and kaolinite. The addition of kaolinite increased the reactivity significantly due to the formation of metakaolin, while the co-calcination also limited the free sodium by binding it in sodium aluminosilicate phases such as nepheline (Danner and Justnes 2020). The replacement of a large fraction (>20 wt%) of cement with the co-calcined BR as SCM was not studied and only a minor replacement resulted in significant strength decrease (Danner and Justnes 2020).

This article develops the co-calcination process further to study its potential for transforming BR into a reactive and robust SCM. The potential of co-calcination is evaluated for a range of BRs from a wide variety of alumina plants. The cause of reactivity is identified and the possibility of tuning the technical and environmental quality criteria is explored, explaining why and how bauxite residue can contribute to the formation of hydration products in a cementitious system.

MATERIALS AND METHODS

Bauxite residues (BRs) from eight alumina plants were investigated. Samples were dried at 105°C until a constant mass was obtained. Afterward, deagglomeration was carried out in a disc mill. The chemical composition of the BRs–given in **Table 1** was measured on glass beads (1.4 g of BR with 12.6 g of lithium borate and lithium bromide flux, prepared at 1,050°C) using quantitative X-ray fluorescence (XRF) using matrix-matched standards by means of a Bruker S8 Tiger WDXRF spectrometer. The loss on ignition from an ambient temperature to 1,000°C was determined using thermal analysis. Portland cement from Holcim (CEM I 52.5 N) and kaolinite from VWR (Bole White) were used.

Particle size distributions were determined using a Horiba LA-350 laser diffractometer. The raw BRs were measured thrice to

TABLE 1 | Chemical composition (major elements, > 1 wt%) of the bauxite residues determined by WD-XRF and loss on ignition by thermal analysis. The information of the Holcim CEM I as delivered by the supplier is added (this cement also includes 1.0 wt% MgO, 0.9 wt% K_2O, and 3.1 wt% SO_3).

BR origin	BR abbreviation	Fe_2O_3 (wt%)	Al_2O_3 (wt%)	SiO_2 (wt%)	Na_2O (wt%)	CaO (wt%)	TiO_2 (wt%)	LOI (wt% TGA)
Alcoa Australia	AlcA	34.9	23.0	13.9	4.8	4.12	1	12
Alcoa Spain	AlcS	53.3	17.2	5.9	4.6	0.8	7.1	9
Alum	Alum	48.7	17.8	8.7	5.2	4.4	3.4	10
Aluminium Oxide Stade	AOS	49.5	11.2	8.0	4.9	5.1	8.3	8
Aughinish Alumina (Rusal)	AAL	47.1	14.2	8.8	4.9	4.1	7.1	8
Hydro	Hyd	37.4	20.8	15.1	8.8	1.2	4.5	7
Mytilineos	Myt	39.6	21.5	8.8	3.6	8.0	5.6	9
Rio Tinto	Rio	50.5	15.1	9.4	5.1	4.5	2.4	8
Holcim	*CEM I*	*2.9*	*5.0*	*20.4*	*0.3*	*64.4*	*0.2*	*1.2*

obtain information on the sample inhomogeneity. The samples were dispersed in isopropanol using ultrasound prior to the measurements. No material comminution was carried out. The phase composition was studied using X-ray diffraction (XRD) on a PANalytical Empyrean with a Co source. Measurements were carried out at 40 kV and 45 mA, using a step size of 0.0131° 2θ and a counting time of 0.02 s/step. An analysis was done using HighScore X'Pert software supported by the PDF-4 database. Quantitative results were obtained from Rietveld refinement using an external rutile standard for the quantification of the amorphous fraction. The external standard was measured maximum 10 days before/after the measurements of the samples. The selected structure files and fitted diffractograms are provided in the supplementary information for the reader's review.

Calcination of the BRs and the mixtures of BR and kaolinite was carried out in a Nabertherm box furnace at 750°C in alumina crucibles, using a dwell time of 1 h and a heating and cooling rate of 3°C/min (the limiting rate for guaranteeing an extensive lifetime of the furnace refractories and heating elements). The calcination produced 500 g of sample per crucible and eight crucibles could fit in one furnace run. The resulting calcined samples were given a name representing the BR source (see **Table 1**) and the BR content in wt%. The presence of kaolinite was indicated using "/K". Example names are Rio100 or Myt70/K, referring to calcined Rio Tinto BR without kaolinite or calcined Mytilineos BR with 30 wt% of kaolinite (70 wt% of BR), respectively. A full overview of the investigated mixtures is provided in the supplementary information (**Supplementary Table S3**). The BRs and kaolinites were manually blended after drying until no color difference was observed in the blend and afterward shaken and turned around in a closed bottle to further homogenize the powder mixture.

The reactivity of the calcined BRs was measured using the R^3 test (ASTM C1897-20). A paste of the calcined BR with excess $Ca(OH)_2$ and a minor amount of $CaCO_3$, K_2SO_4, and KOH is mixed and introduced into the isothermal calorimeter. The materials were stored at 40°C overnight before mixing and the measurements were carried out at 40°C for 7 days. An R^3 paste mixture with lower a liquid/solid and $Ca(OH)_2$/BR ratio was mixed to study the reactive components of the calcined BR. This mixture was hydration stopped—according to the RILEM-recommended procedure using solvent exchange with isopropanol and diethylether (Snellings et al., 2018) - after curing for 7 days at 40°C and studied using SEM and XRD. For SEM, the hardened paste samples were embedded in epoxy resin, polished, and coated with Pt. Backscattered electron images and EDS mappings were taken in a FEI Nova NanoSEM 450. Additional calorimetry measurements to study the kinetics of hydration were carried out on cement pastes composed of 70 wt% of the CEM I and 30 wt% of calcined BR using a water/solid ratio of 0.5. These measurements were carried out for 28 days at 20°C.

The performance properties and environmental compatibility of the co-calcined BRs as SCM were investigated by making mortars according to EN 196–1 with 30 wt% substitution of the CEM I by the SCMs. Master Glenium 51 superplasticizer (PCE, 35 wt% active content) was added to reach the same mortar flow (measured according to EN 1015–3) as a CEM I reference sample. The compressive strength was measured according to EN 196–1 at days 2, 7, and 28 (on 4 samples per mixture per day) and batch-leaching tests were carried out on the broken mortars after 28 days according to EN 12457–2 simulating the end-of-life scenario and the environmental requirements for the second life of concrete.

RESULTS AND DISCUSSION

Characteristics of the Raw and Calcined Bauxite Residues

BR is a fine material. After deagglomeration, the d_{50} of all received samples was <10 μm (**Table 2**). Most samples have a d_{50} of about 3 μm, apart from those originating from the Alcoa factories. These values are in line with published observations (Ribeiro and Morelli 2011; Manfroi et al., 2014; Romano et al., 2018). Apart from the Alcoa samples, the variation between BRs is limited across all percentiles. The minor variations observed are similar to batch-to-batch variability and sample inhomogeneity (the latter was experimentally confirmed). The calcination process does not have a significant or consistent effect on the particle size distribution. Therefore, there would be no need for milling after the calcination process.

The quantities of the detected phases are given in detail in **Supplementary Table S2** (supplementary information) for the

TABLE 2 | Percentiles of the particle size distribution of the BRs before and after calcination.

BR	d_{10} (µm, before/after calcination)	d_{50} (µm, before/after calcination)	d_{90} (µm, before/after calcination)
AlcA	1.2/1.2	8.8/7.3	53.6/43.2
AlcS	0.7/0.6	9.0/5.5	72.3/38.7
Alum	1.0/0.9	3.7/3.0	22.9/26.6
AOS	0.5/0.6	2.5/3.3	21.3/22.1
AAL	0.7/0.6	3.0/3.3	19.3/39.3
Hyd	0.9/1.2	3.8/4.4	20.2/15.3
Myt	0.5/0.8	2.9/4.9	12.0/31.6
Rio	0.6/0.7	3.3/3.1	22.0/27.6

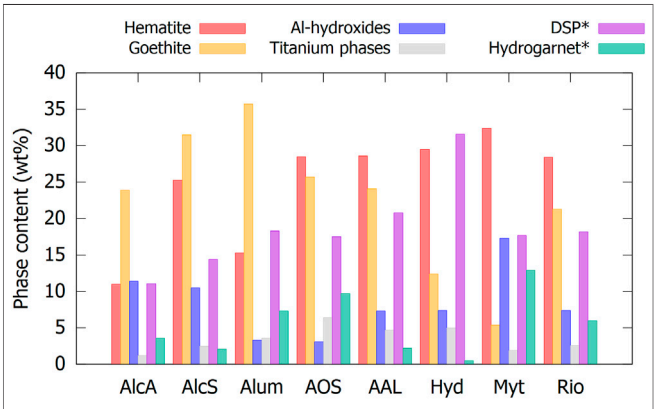

FIGURE 1 | Quantification of the major phases in the raw BRs. *the quantity of DSP and hydrogarnet also takes into account the calculated amount of nano-crystalline DSP and hydrogarnet.

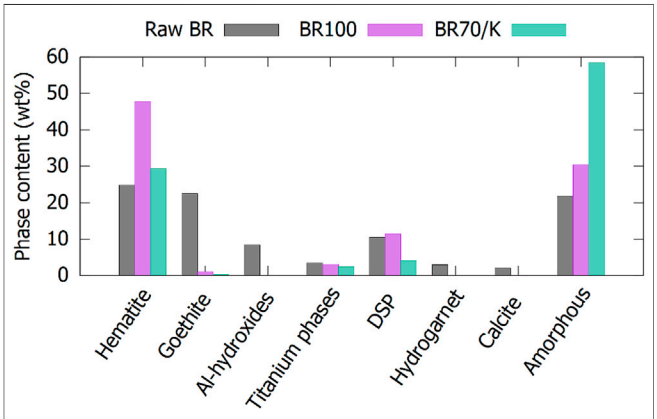

FIGURE 2 | Quantification of the major phases in raw, calcined, and co-calcined BRs. The results are averaged over the eight different origins of the BRs. Only the crystalline part of the DSP and hydrogarnet is taken into account.

raw BRs, the calcined BR100s and the co-calcined BR70/Ks are visualized in **Figure 1** for the raw BRs. A rough estimation of the nano-crystalline structures not detected by XRD was made based on mass–balance calculations using the XRF data (for Si and Ca) from **Table 1**. This is only carried out for the raw BRs before calcination. The Ca not found in crystalline phases was attributed to nano-crystalline hydrogarnet, the remaining Si not found in crystalline phases or nano-crystalline hydrogarnet was used to calculate the nano-crystalline DSP (desilication products; sodalite or cancrinite). The nano-crystalline hydroxides were calculated by subtraction from the total XRD amorphous. No distinction is made between Fe-hydroxides or Al-hydroxides, as it is not possible to provide a trustworthy result due to the extensive solubility of Al and other elements in the goethite phase and the associated difficulties in the Al and Fe mass balance.

The major crystalline phases in BR can be grouped into four main categories: iron-containing phases, aluminum hydroxides, DSP, and titanium-containing phases. The iron-containing phases are hematite and goethite and comprise the largest part of the BR (50–70 wt%). Significant solid solutions can occur in the hematite and goethite phases; especially, Al, Cr, and Ti can substitute Fe in the structure (Gräfe et al., 2011; Gräfe et al., 2017). This was also observed in the present results. The ratio of the intensity of the 111 to that of the 110 peak of goethite suggests a significant substitution of Fe for Al (Ford et al., 1997). The diffractogram could best be fitted by modeling the goethite as $Fe_{0.8}Al_{0.2}OOH$. A variety of aluminum hydroxide phases are present, which usually make up 5–10 wt% of the BR, but can range from 2 to 15 wt % (Gräfe et al., 2011; Gräfe et al., 2017). The DSP is either sodalite or cancrinite, although a combination can also be present. Hydrogarnet could also be considered a product of desilication, but is usually present at a lower concentration and is not counted within the DSP phases. In total, DSP phases can amount to 11–32 wt% of the BR when also counting the amorphous fraction. Comparing specific BRs to the literature that has previously investigated a sample from the same source, the values correspond well. For example, Hydro BR was previously investigated by (Danner and Justnes 2020), Mytilineos BR by (Hertel et al., 2016), and Aughinish Alumina BR by (Hertel et al., 2019).

During (co-)calcination, the hydroxides transform into oxides. The increase in hematites is clearly observed in **Figure 2**, but aluminum oxides were not detected for most of the calcined BRs. Only in Myt100, corundum was detected (**Supplementary Table S2** in supplementary information), the rest of the aluminum oxides probably were XRD amorphous. Titanium-containing phases remained relatively stable during

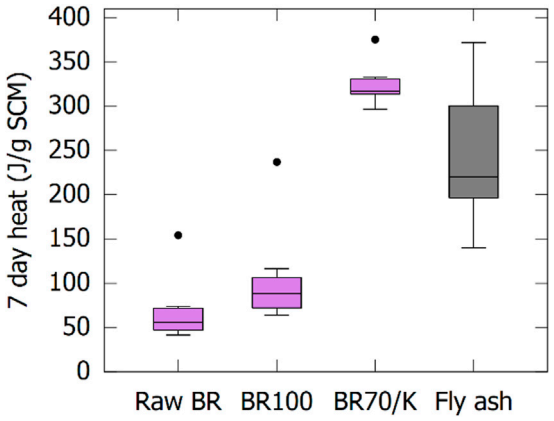

FIGURE 3 | Boxplots giving the cumulative heat at 7 days in the R³ test of BR before and after (co-)calcination.

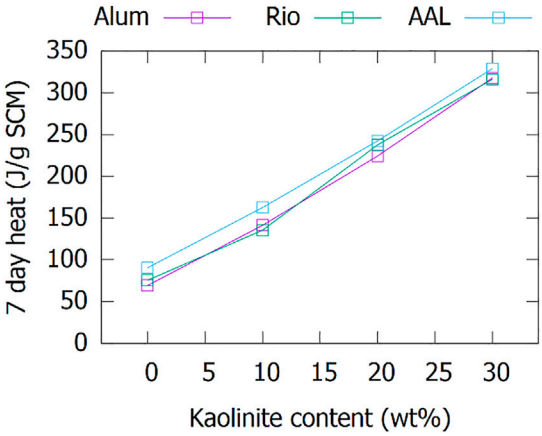

FIGURE 4 | Variation with a kaolinite replacement of BR before calcination of the cumulative heat at 7 days in the R³ test.

(co-)calcination. Calcite and muscovite/illite were significantly lowered during calcination, but complete decomposition was not achieved. No free limes were detected in the calcined materials, so it is expected that the Ca from calcite was incorporated in the XRD amorphous phases. Complete decomposition of the hydrogarnet phase and the minor content of kaolinite occurred during calcination. Only in Myt100, a clear crystalline reaction product from the calcined hydrogarnet was identified, as the Myt BR is the one with the highest hydrogarnet content, by far. A garnet phase with similar lattice parameters as the hydrogarnet was observed. The hydrogarnet lost water, but the structure was not completely destroyed. The DSP content stayed relatively stable during calcination (BR100) or even a slight increase could be noticed due to the crystallization of a part of the XRD amorphous DSP. However, the co-calcination process (BR70/K) significantly lowered the DSP content. During calcination (BR100), some of the Na is bound in nepheline in five of the eight BRs, while after co-calcination, no nepheline was detected (BR70/K), instead a very low amount of albite could be fitted to the diffractograms. No clear peaks of albite were detected, but the quality of the fittings was improved by the addition of a broad albite signal. In isolated cases, kalsilites or alunites were detected after calcination. In general, the amorphous content was increased by the calcination process, but an estimation of the nature and quantities of the nano-crystalline phases based on mass balance could not be made. The differences from calcined BR100 to co-calcined BR70/K have to be interpreted in light of the addition of roughly 30 wt% of metakaolinite. The phases that decreased in quantity significantly more than the expected dilution effect were the DSP phases. In case of the Mytilineos BR, there might also have been a decrease for the grossular garnet. These decompositions occurred at the benefit of additional XRD amorphous content on top of the 30 wt% of metakaolinite. The combination of metakaolinite and DSP at a high temperature led to an interaction decomposing the crystalline DSP and forming an XRD amorphous phase.

Reactivity of Calcined Bauxite Residues

The reactivity of all eight BRs is evaluated before calcination, after calcination (BR100), and after co-calcination with 30 wt % of kaolinite (BR70/K) using the R³ test. The cumulative heat after 7 days is reported in boxplots in **Figure 3**. The variation in the reactivity between BR sources was limited, apart from one outlier for each boxplot, which is always the sample based on Hydro BR. The raw BRs and BR100s have a low reactivity, although the reactivity increased slightly for all BRs. This small increase in reactivity by calcination has been observed before (Ribeiro et al., 2013; Manfroi et al., 2014). A large increase in reactivity is observed after co-calcination with kaolinite. The co-calcined BR70/K samples have a medium–high reactivity, comparable to high-quality coal fly ashes (see **Figure 3**, the 25th percentile of the BR70/K is higher than the 75th percentile of the fly ashes). Furthermore, the variation in reactivity of the different co-calcined samples is much lower than the variation in reactivity of coal fly ashes, despite the different origins of the BRs. In other words, on top of having a higher reactivity than the average fly ash, which was also shown recently (Danner and Justnes 2020), the co-calcined BR is more robust in terms of reactivity than coal combustion fly ashes and relatively independent from the refinery of origin. The cumulative heat of the calcined samples after 7 days is also comparable to the heat recorded of some slags produced via partial vitrification of BR (Giels et al., 2022; Hertel et al., 2022).

Having a reactivity higher than fly ashes might not be needed for many cement and concrete applications. The co-calcination with varying kaolinite contents is therefore investigated in more detail for a random selection of three BRs. The cumulative heat depicted in **Figure 4** shows an approximately linear relationship with the kaolinite content in the feed for calcination for the three studied BRs. The

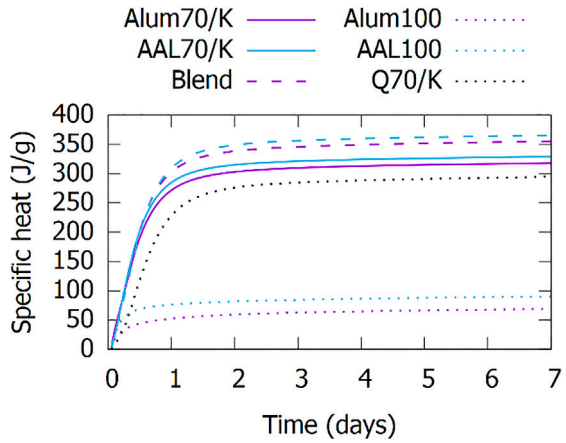

FIGURE 5 | Comparison between co-calcined BR and reference mixtures.

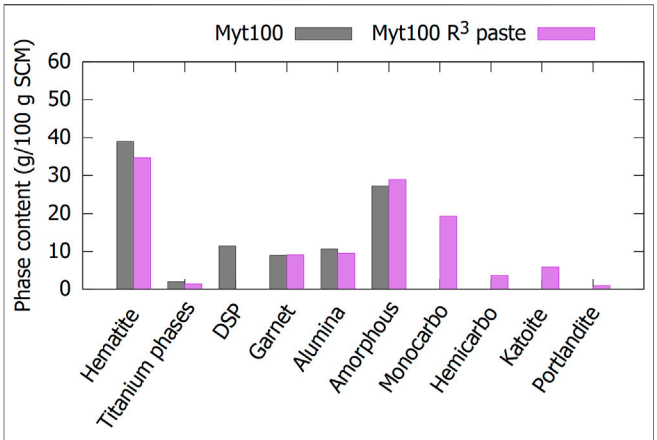

FIGURE 6 | Quantification of the major phases in the calcined Mytilineos BR and the reacted R^3-like paste made from it. Only the crystalline part of the DSP and hydrogarnet is taken into account.

reactivity can, thus, simply be chosen and controlled by the wt % kaolinite addition to the bauxite residue before calcination.

The results in **Figure 3** and **Figure 4** raise the question of why BR should be added to metakaolin if metakaolin is contributing most to the reactivity. Apart from the obvious price advantage of BR vs pure kaolinite and the residue valorization/upcycling aspect, BR does contribute to increase the quality of the SCM after calcination. With respect to reactivity, this becomes clear when comparing the co-calcined BR70/K to fine quartz filler (Sibelco M400, d_{50} = 12 µm) co-calcined with 30 wt% of kaolinite (Q70/K, **Figure 5**). A small but significant contribution to the reactivity is made; however, the increase in reactivity is lower than that of the corresponding share of calcined BR100 sample.

To identify the phase in BR to which the reactivity should be attributed, an R^3-like paste is mixed from sample AAL100 (see **section 2** for the detailed description of the synthesis procedure). The hydration of this paste is studied using XRD to quantify the reaction extent of the crystalline phases. The phase composition of the reacted paste was recalculated to the SCM content to have the same basis of comparison. The only significant decrease from SCM to the hydrated paste in **Figure 6** is the DSP phase (cancrinite in the case of Myt BR), which completely reacted. The iron oxides, titanium-containing phases, garnet, and alumina phases did not react significantly. The phases that are new or increased in content are the products of reaction of the SCM with the R^3 mixture-containing portlandite. These reaction products are monocarboaluminate, katoite, C-S-H, and XRD amorphous phase(s). The quantification of the amorphous phases included the quantity of C-S-H.

The XRD amorphous nano-crystalline DSP should have a similar (or slightly higher) reactivity as its crystalline equivalent. Confirmation of the low reactivity of the dehydroxylated Al-hydroxides was obtained from microchemical investigations. The SEM image and elemental EDS maps of the hydrated R^3-like paste in **Figure 7** shows particles which are pure Al (oxygen was not included in the figure, but was present in the complete image). Most images taken using SEM contained such alumina particles. The nano-crystalline alumina does not react extensively.

Co-Calcined Bauxite Residue as a Robust Supplementary Cementitious Material

Mortar mixtures were made by replacing 30 wt% of the CEM I with (co-)calcined BR. A constant workability at equal water/binder mass ratio was aimed for. Therefore, superplasticizer was added to reach the same mortar flow as the CEM I reference mortar. The required superplasticizer dosage to reach this reference flow is shown in **Figure 8**. Based on the literature, a decrease in workability or increase in superplasticizer demand was expected for the mortars including the SCM (Ribeiro et al., 2010; Tang et al., 2019). Co-calcination with kaolinite did not lower the average superplasticizer requirement, but the variation with the BR source on the result was significantly reduced. This suggests a change in the mechanism that lowers the workability. For BR, the decreased workability is correlated with the soluble sodium level of the BR (Ribeiro et al., 2010; Tang et al., 2019). This correlation is weakened for the co-calcined BRs as the free sodium is significantly decreased by the co-calcination process (see **Supplementary Table S4** and (Danner and Justnes 2020)). However, metakaolin and calcined clays also decrease the workability of mortars and concretes, because of the intricate particle morphology and the associated high specific surface area (Tregger et al., 2010; Scrivener et al., 2019). As can be seen from the comparison with the co-calcined quartz (Q70/K) in **Figure 8**, the BR itself did not contribute as extensively to the increased superplasticizer requirement as for the BR100 samples, and about half of the workability loss can be attributed to the metakaolin. The limited increase in superplasticizer requirement of the BR70/K-containing samples in comparison with the samples with co-calcined quartz filler is likely related to a combined effect of the fineness of the BR (dominant) and a minor amount of residual soluble sodium (subordinate).

The free sodium does not only have an effect on the flow at an early age, but also on the hydration kinetics of the blended cement pastes. The calcined BR100 samples can result in a strong acceleration of the cement hydration. In **Figure 9**, this is clear for Alum100: a significant amount of heat flow is already occurring at the start of the measurement, this high initial heat peak is followed by a significantly delayed main

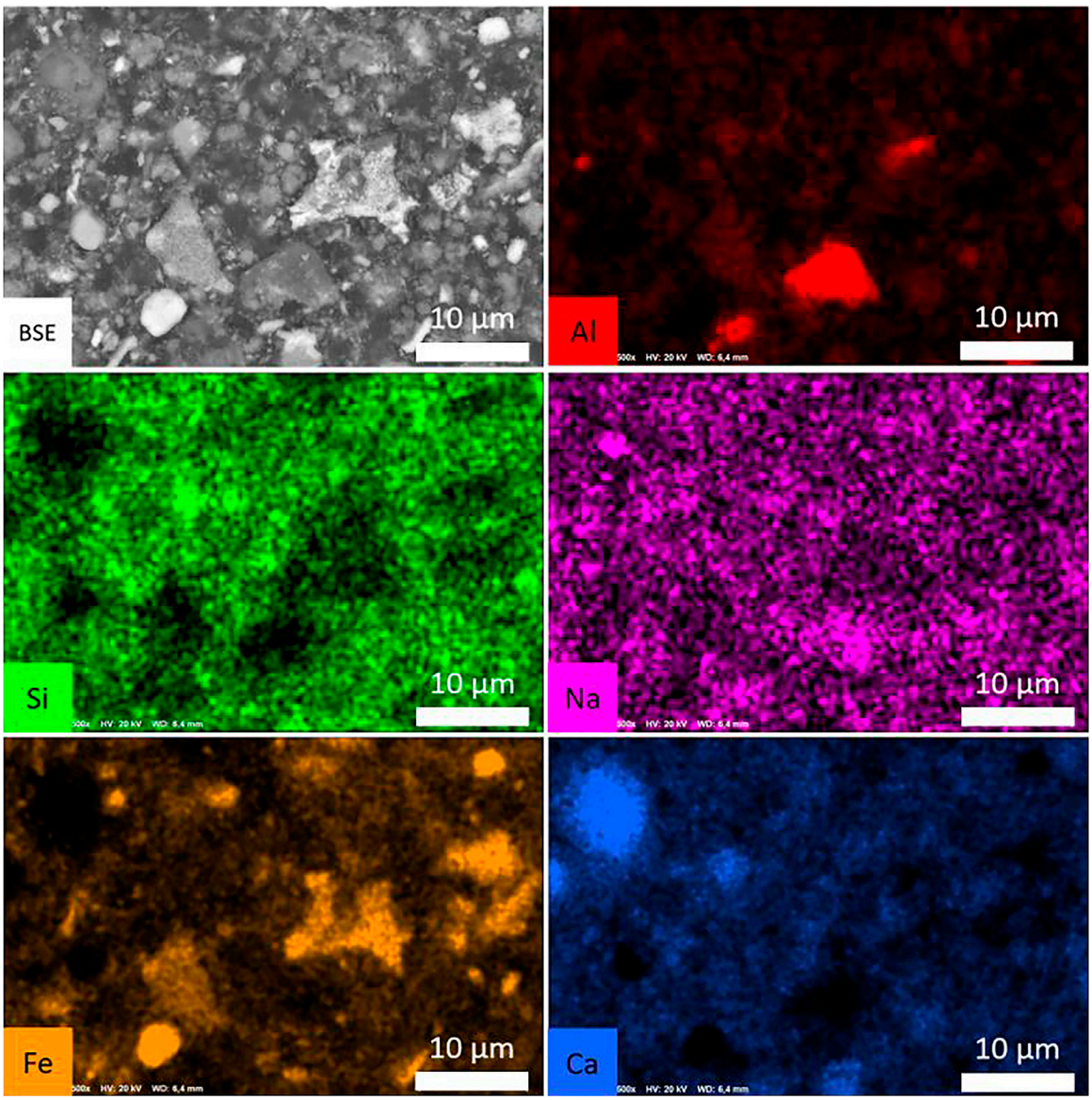

FIGURE 7 | SEM image and elemental maps of the reacted R³-like paste.

hydration peak. Macroscopically, the high initial heat peak translated in fast setting of the sample, immediately (15–30 min) after mixing. This effect is not observed for the AAL100. Alum BR has the highest soluble sodium content amongst all tested BR; therefore the high initial heat flow peak is likely related to the free sodium in this particular sample and the associated washing process at the alumina refinery. Co-calcination neutralizes the accelerating effect of free sodium. The perturbing effect on the kinetics of cement hydration is already overcome by the addition of 10 wt% of kaolinite before calcination. The extreme cases of the eight studied BRs are shown in **Figure 9**. The BRs from other sources, as well as previous results ((Danner and Justnes 2020) and (Ribeiro et al., 2013)) showed a behavior in between the two presented. The avoidance of severe acceleration from 10 wt% of kaolinite shows that already a minor amount of kaolinite added before calcination results in an interaction during calcination enabling it to bind most of the free sodium in the BR.

The compressive strengths of the mortars are presented in **Figure 10** as the mortar relative strength of material X by comparison with the CEM I reference at the same curing age ($strength_X/strength_{CEM\ I}$ x 100%). This reference mortar reached 37, 50, and 61 MPa at 2, 7, and 28 days of curing age, respectively. The acceleration that occurred for the BR100 samples due to the soluble sodium content was also reflected in the compressive strength at 2 days. All samples showed higher early strengths than a reference mortar with 30 wt% of co-calcined quartz filler (Q70/K). This early age acceleration effect is less apparent for the

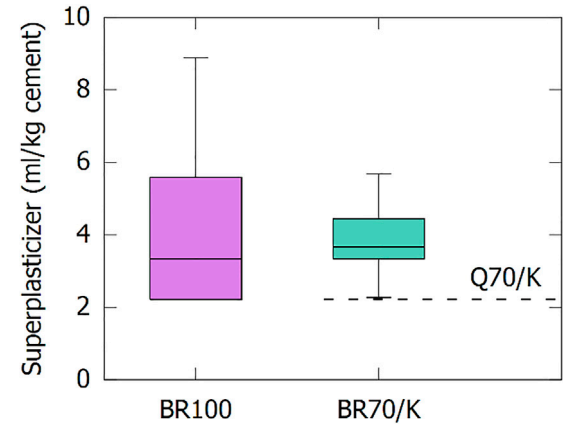

FIGURE 8 | Superplasticizer requirement of the mortars including (co-) calcined BR as SCM. The dashed line indicates the superplasticizer requirement of quartz co-calcined with 30 wt% of kaolinite.

mortars containing co-calcined BR (BR70/K samples). However, at days 7 and 28, the strength of the BR70/K samples approached the CEM I reference sample (85–90%) indicating a significant activity of the co-calcined BRs and aligning with the R^3 reactivity test results. In contrast, the strength of most of the BR100 samples at a later age was lower than the inert filler. The strength gain slowed down significantly due to a lack of reactivity and the well-known negative effects of alkalis on long-term strength development of Portland cements (Mota et al., 2018). The strengths of the mortars with 30 wt% co-calcined BR fall within the 42.5 R strength class defined in EN 197–1. In comparison with the values presented by (Danner and Justnes 2020), the strengths were significantly higher despite the higher replacement level used here. This may be related to the somewhat different calcination procedure, using lower temperatures (Danner and Justnes 2020), resulting in less transformation of reactive metakaolin into relatively inert sodium aluminosilicate phases. Another important difference was the procedure for

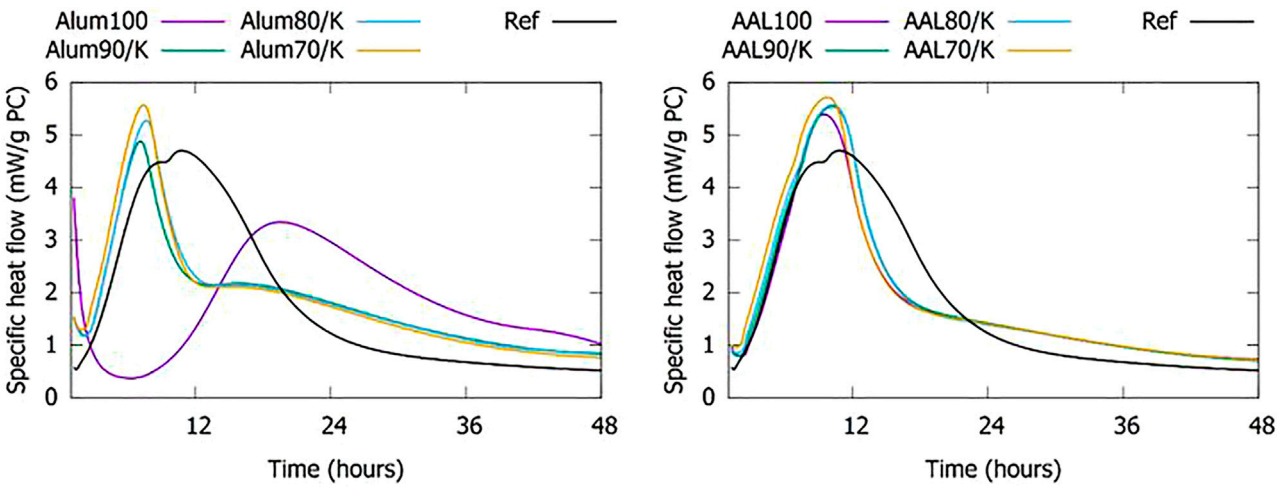

FIGURE 9 | Heat flow from pastes with 70 wt% of CEM I and 30 wt% of (co-)calcined BR. The reference sample (Ref) shows the heat flow of a paste with 70 wt% of CEM I and 30 wt% of quartz filler.

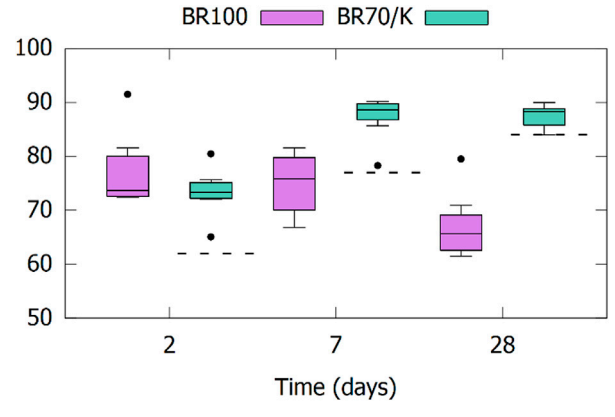

FIGURE 10 | Compressive strength of mortars with 30 wt% of (co-) calcined BR as SCM relative to a reference sample of the CEM I. The dashed lines indicate the relative strengths of a mortar with co-calcined quartz Q70/K as a basis of comparison for the BR70/K samples.

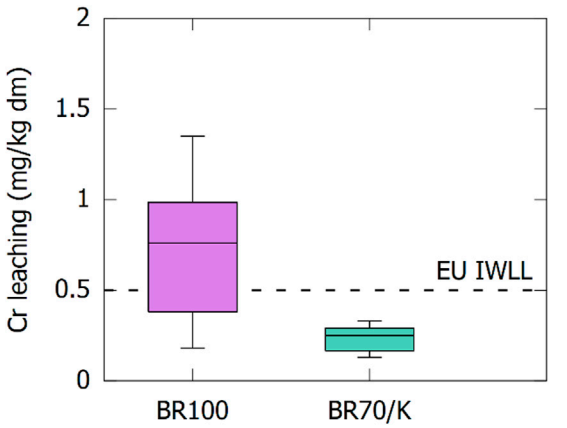

FIGURE 11 | Concentration of Cr in the leachate after batch-leaching in mg/kg dry matter. The leaching of the mortars after 28 days is compared with the EU inert waste leaching limit (IWLL).

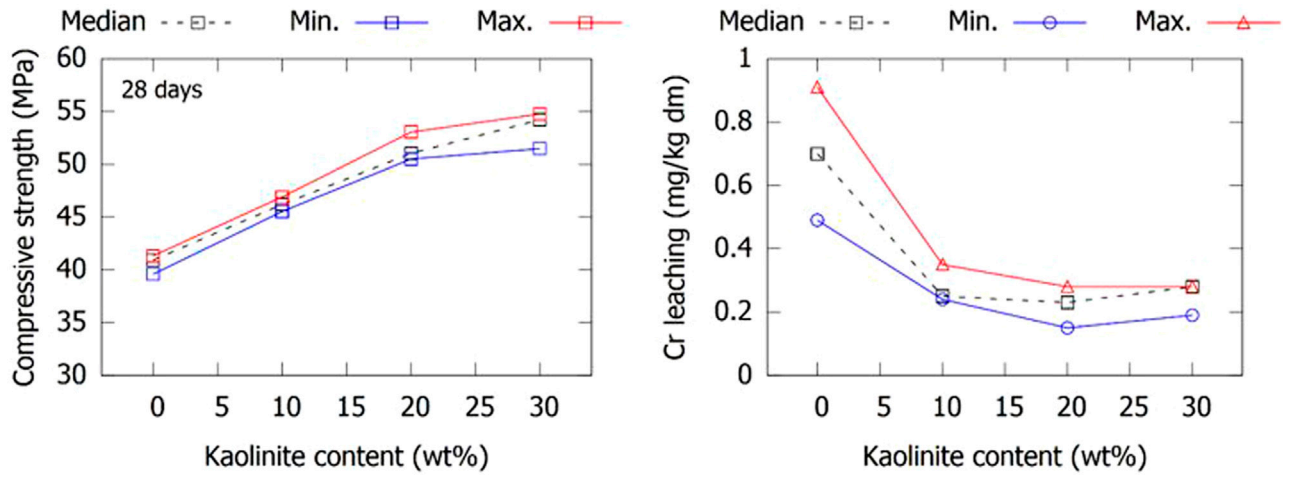

FIGURE 12 | The variation with kaolinite addition to BR before calcination of the compressive strength and chromium leaching of mortars after 28 days.

mortar mixing, where (Danner and Justnes 2020) did not add a superplasticizer, which might have caused a low workability of the mortar and increased porosity or molding defects of the mortar test samples.

In addition to the mechanical performance, the use of cements including waste materials has to be subjected to an assessment of environmental compatibility. Here, we focus on the mobility of heavy metals contributed by the BR. The crushed mortars obtained from the 28 days of strength testing were subjected to a batch-leaching test, and the leachate was analyzed for heavy metals. Even though BRs might contain As, V, or other metals and metalloids (Evans 2016; IAI 2020), from the BRs studied in this article, only Cr was detected in concentrations close to the legislative limits for leaching. **Figure 11** shows that most mortars including calcined BR (without kaolinite) did not comply with the European inert waste leaching limits (IWLL). When the BR was co-calcined with 30 wt% of kaolinite, all mortars complied.

The compressive strength and Cr leaching of mortars were also investigated for co-calcined BRs with lower levels of kaolinite (10 and 20 wt%). The 28 days strength and Cr leaching of the mortars for the three selected BR sources is shown in **Figure 12**. Similar to the reactivity results in **Figure 4**, the 28 days strength linearly increased with the kaolinite level. Although a perfectly linear relationship is not observed for all BR samples, the results still allow an accurate prediction of the strength development using the kaolinite content. The Cr leaching is significantly reduced with minor kaolinite additions and 10 wt% seems to be sufficient for lowering the leached Cr value to be under the IWLL. The good technical and environmental performance with low kaolinite contents opens a pathway to the use of low-grade kaolinitic clays, which are currently sourced for the production of LC^3 cements by many cement manufacturers. The use of such clays with around 40 wt% of kaolinite (Scrivener et al., 2018) would greatly increase the economic feasibility of the co-calcination process and–if the desired technical and environmental results are maintained–pave the way towards industrial implementation.

CONCLUSION

In an attempt to match the availability of bauxite residues and the need for high-volume SCMs, a co-calcination process was proposed and investigated in this article. The performance of co-calcined bauxite residue and kaolinite at 750°C for use as SCM was assessed using bauxite residues from eight alumina refineries. SCMs with a moderate/high reactivity were obtained when co-calcining 30 wt% of kaolinite with 70 wt% of the bauxite residue. The reactivity can be adapted using the wt% of kaolinite in the blend. The inherent reactivity of the bauxite residue mostly originated from desilication products such as sodalite and cancrinite, as observed from the phase composition of an R^3-like paste after curing. During co-calcination, the sodium-containing phases reacted with the kaolinite/metakaolinite phase, decreasing the soluble sodium in the calcined product.

The contribution to strength development of mortars incorporating 30 wt% of SCM was related to the kaolinite content in a similar way as the reactivity. The reactivity and strength development did not vary substantially with varying bauxite residue sources. The presence of soluble sodium in the bauxite residue additionally increased the early strength of the mortar, but negatively affected the later age strength. The workability of the mortars was slightly decreased by the addition of (co-)calcined bauxite residue, although excessive acceleration of the hydration reactions and fast setting could be avoided by use of 10 wt% of kaolinite in the co-calcination blend (or more). The co-calcination with kaolinite also decreased the leaching of Cr from the mortars and lowered the values below the EU inert waste leaching limit already at 10 wt% of co-calcined kaolinite.

DATA AVAILABILITY STATEMENT

The original contributions presented in the study are included in the article/**Supplementary Material**; further inquiries can be directed to the corresponding author.

AUTHOR CONTRIBUTIONS

Conceptualization: AP and RS. Methodology: AP and TH. Formal analysis: AP. Writing: AP TH, and RS. Review and editing: RS and TH. Supervision: RS.

FUNDING

The research leading to these results has been performed within the REACTIV project and received funding from the European Community's Horizon 2020 Programme (H2020/2014-2020) under grant agreement no. 958208.

ACKNOWLEDGMENTS

The authors are thankful to the alumina plants and Holcim for providing the materials that made this study possible. Special thanks go out to the VITO lab technicians for carrying out the experiments.

SUPPLEMENTARY MATERIAL

The Supplementary Material for this article can be found online at: https://www.frontiersin.org/articles/10.3389/fmats.2022.913151/full#supplementary-material

REFERENCES

Aubert, J., Husson, B., and Sarramone, N. (2006). Utilization of Municipal Solid Waste Incineration (MSWI) Fly Ash in Blended cementPart 1: Processing and Characterization of MSWI Fly Ash. *J. Hazard. Mater.* 136 (3), 624–631. doi:10.1016/j.jhazmat.2005.12.041

Bouchikhi, A., Benzerzour, M., Abriak, N.-E., Maherzi, W., and Mamindy-Pajany, Y. (2019). Study of the Impact of Waste Glasses Types on Pozzolanic Activity of Cementitious Matrix. *Constr. Build. Mater.* 197, 626–640. doi:10.1016/j.conbuildmat.2018.11.180

CEMBUREAU (2020). Key Facts & Figures. Available at: https://cembureau.eu/about-our-industry/key-facts-figures/.

Danner, T., and Justnes, H. (2020). Bauxite Residue as Supplementary Cementitious Material - Efforts to Reduce the Amount of Soluble Sodium. *Nordic Concr. Res.* 62 (1), 1–20. doi:10.2478/ncr-2020-0001

Evans, K. (2016). The History, Challenges, and New Developments in the Management and Use of Bauxite Residue. *J. Sustain. Metall.* 2 (4), 316–331. doi:10.1007/s40831-016-0060-x

Ford, R. G., Bertsch, P. M., and Seaman, J. C. (1997). Goethite Morphologies Investigated via X-Ray Diffraction of Oriented Samples. *Clays Clay Minerals* 45 (5), 769–772. doi:10.1346/ccmn.1997.0450515

Garside, M. (2021). Cement Production Worldwide from 1995 to 2020. Available at: https://www.statista.com/statistics/1087115/global-cement-production-volume/.

Giels, M., Hertel, T., Gijbels, K., Schroeyers, W., and Pontikes, Y. (2022). High Performance Mortars from Vitrified Bauxite Residue; the Quest for the Optimal Chemistry and Processing Conditions. *Cem. Concr. Res.* 155, 106739. doi:10.1016/j.cemconres.2022.106739

Gräfe, M., Klauber, C., McFarlane, A. J., and Robinson, D. J. (2017). *Clays in the Minerals Processing Value Chain*. Cambridge University Press.

Gräfe, M., Landers, M., Tappero, R., Austin, P., Gan, B., Grabsch, A., et al. (2011). Combined Application of QEM-SEM and Hard X-Ray Microscopy to Determine Mineralogical Associations and Chemical Speciation of Trace Metals. *J. Environ. Qual.* 40 (3), 767–783.

Habert, G., Miller, S. A., John, V. M., Provis, J. L., Favier, A., Horvath, A., et al. (2020). Environmental Impacts and Decarbonization Strategies in the Cement and Concrete Industries. *Nat. Rev. Earth Environ.* 1 (11), 559–573. doi:10.1038/s43017-020-0093-3

Hallet, V., De Belie, N., and Pontikes, Y. (2020). The Impact of Slag Fineness on the Reactivity of Blended Cements with High-Volume Non-ferrous Metallurgy Slag. *Constr. Build. Mater.* 257, 119400. doi:10.1016/j.conbuildmat.2020.119400

Hertel, T., Blanpain, B., and Pontikes, Y. (2016). A Proposal for a 100 % Use of Bauxite Residue towards Inorganic Polymer Mortar. *J. Sustain. Metall.* 2 (4), 394–404.

Hertel, T., Novais, R. M., Murillo Alarcón, R., Labrincha, J. A., and Pontikes, Y. (2019). Use of Modified Bauxite Residue-Based Porous Inorganic Polymer Monoliths as Adsorbents of Methylene Blue. *J. Clean. Prod.* 227, 877–889. doi:10.1016/j.jclepro.2019.04.084

Hertel, T., Van den Bulck, A., Blanpain, B., and Pontikes, Y. (2022). Correlating the Amorphous Phase Structure of Vitrified Bauxite Residue (Red Mud) to the Initial Reactivity in Binder Systems. *Cem. Concr. Compos.* 127, 104410. doi:10.1016/j.cemconcomp.2022.104410

IAI (2020). *Technology Roadmap: Maximising the Use of Bauxite Residue in Cement*.

IAI (2021). World Aluminium - Statistics. Available at: https://international-aluminium.org/statistics/alumina-production/.

Juenger, M. C. G., Snellings, R., and Bernal, S. A. (2019). Supplementary Cementitious Materials: New Sources, Characterization, and Performance Insights. *Cem. Concr. Res.* 122, 257–273. doi:10.1016/j.cemconres.2019.05.008

Manfroi, E. P., Cheriaf, M., and Rocha, J. C. (2014). Microstructure, Mineralogy and Environmental Evaluation of Cementitious Composites Produced with Red Mud Waste. *Constr. Build. Mater.* 67, 29–36. doi:10.1016/j.conbuildmat.2013.10.031

Mladenovič, A., Mirtič, B., Meden, A., and Zalar Serjun, V. (2016). Calcium Aluminate Rich Secondary Stainless Steel Slag as a Supplementary Cementitious Material. *Constr. Build. Mater.* 116, 216–225.

Monteiro, P. J. M., Miller, S. A., and Horvath, A. (2017). Towards Sustainable Concrete. *Nat. Mater* 16 (7), 698–699. doi:10.1038/nmat4930

Mota, B., Matschei, T., and Scrivener, K. (2018). Impact of NaOH and Na2SO4 on the Kinetics and Microstructural Development of White Cement Hydration. *Cem. Concr. Res.* 108, 172–185. doi:10.1016/j.cemconres.2018.03.017

Ohenoja, K., Wigren, V., Österbacka, J., and Illikainen, M. (2019). Applicability of Fly Ash from Fluidized Bed Combustion of Peat, Wood, or Wastes to Concrete. *Waste Biomass Valor* 10 (11), 3525–3534. doi:10.1007/s12649-018-0319-5

Pamenter, S., and Myers, R. J. (2021). Decarbonizing the Cementitious Materials Cycle: A Whole-systems Review of Measures to Decarbonize the Cement Supply Chain in the UK and European Contexts. *J. Industrial Ecol.* 25 (2), 359–376. doi:10.1111/jiec.13105

Peys, A., Košir, M., Snellings, R., Mladenovič, A., and Horckmans, L. (2021). Detoxified Spent Pot Lining from Aluminum Production as (Alumino-)Silicate Source for Composite Cement and AutoClaved Aerated Concrete. *Appl. Sci.* 11 (8), 3715. doi:10.3390/app11083715

Power, G., Gräfe, M., and Klauber, C. (2011). Bauxite Residue Issues: I. Current Management, Disposal and Storage Practices. *Hydrometallurgy* 108 (1), 33–45. doi:10.1016/j.hydromet.2011.02.006

Ribeiro, D. V., Labrincha, J. A., and Morelli, M. R. (2010). Use of Red Mud as Addition for Portland Cement Mortars. *J. Mater. Sci. Eng.* 4 (8).

Ribeiro, D. V., and Morelli, M. R. (2011). "Use of Red Mud as Addition for Portland Cement Mortars," in 55e Congresso Brasilieiro de Ceramica, Brasil (Porto de Galinhas), 1333–1345.

Ribeiro, D. V., Silva, A. S., Labrincha, J. A., and Morelli, M. R. (2013). Rheological Properties and Hydration Behavior of Portland Cement Mortars Containing Calcined Red Mud. *Can. J. Civ. Eng.* 40 (6), 557–566. doi:10.1139/cjce-2012-0230

Romano, R. C. O., Bernardo, H. M., Maciel, M. H., Pileggi, R. G., and Cincotto, M. A. (2018). Hydration of Portland Cement with Red Mud as Mineral Addition. *J. Therm. Anal. Calorim.* 131 (3), 2477–2490. doi:10.1007/s10973-017-6794-2

Scrivener, K., Avet, F., Maraghechi, H., Zunino, F., Ston, J., Hanpongpun, W., et al. (2019). Impacting Factors and Properties of Limestone Calcined Clay Cements (LC3). *Green Mater.* 7 (1), 3–14. doi:10.1680/jgrma.18.00029

Scrivener, K. L., John, V. M., and Gartner, E. M. (2016). *Eco-efficient Cements: Potential, Economically Viable Solutions for a low-CO_2, Cement-Based Materials Industry. UNEP Report*. Paris: United Nations Environment Programme, 50.

Scrivener, K., Martirena, F., Bishnoi, S., and Maity, S. (2018). Calcined Clay Limestone Cements (LC3). *Cem. Concr. Res.* 114, 49–56. doi:10.1016/j.cemconres.2017.08.017

Serdar, M., Biljecki, I., and Bjegović, D. (2017). High-Performance Concrete Incorporating Locally Available Industrial By-Products. *J. Mater. Civ. Eng.* 29 (3), 04016239. doi:10.1061/(asce)mt.1943-5533.0001773

Simonsen, A. M. T., Solismaa, S., Hansen, H. K., and Jensen, P. E. (2020). Evaluation of Mine Tailings' Potential as Supplementary Cementitious Materials Based on Chemical, Mineralogical and Physical Characteristics. *Waste Manag.* 102, 710–721. doi:10.1016/j.wasman.2019.11.037

Snellings, R., Chwast, J., Cizer, Ö., De Belie, N., Dhandapani, Y., Durdzinski, P., et al. (2018). Report of TC 238-SCM: Hydration Stoppage Methods for Phase Assemblage Studies of Blended Cements—Results of a Round Robin Test. *Mater. Struct.* 51 (4), 1–12. doi:10.1617/s11527-018-1237-5

Tang, W. C., Wang, Z., Donne, S. W., Forghani, M., and Liu, Y. (2019). Influence of Red Mud on Mechanical and Durability Performance of Self-Compacting Concrete. *J. Hazard. Mater.* 379, 120802. doi:10.1016/j.jhazmat.2019.120802

Taylor, K. (2021). *Europe Halfway towards Closing All Coal Power Plants by 2030*. Euractiv. Euractiv.com.

Tregger, N. A., Pakula, M. E., and Shah, S. P. (2010). Influence of Clays on the Rheology of Cement Pastes. *Cem. Concr. Res.* 40 (3), 384–391. doi:10.1016/j.cemconres.2009.11.001

Venkatesh, C., Ruben, N., and Chand, M. S. R. (2020). Red Mud as an Additive in Concrete: Comprehensive Characterization. *J. Korean Ceram. Soc.* 57 (3), 281–289. doi:10.1007/s43207-020-00030-3

Conflict of Interest: The authors declare that the research was conducted in the absence of any commercial or financial relationships that could be construed as a potential conflict of interest.

Publisher's Note: All claims expressed in this article are solely those of the authors and do not necessarily represent those of their affiliated organizations, or those of the publisher, the editors, and the reviewers. Any product that may be evaluated in this article, or claim that may be made by its manufacturer, is not guaranteed or endorsed by the publisher.